Draft version September 22, 2014
Preprint typeset using LaTeX style emulateapj v. 04/17/13

THE DEPENDENCE OF SPIRAL DISK MORPHOLOGY ON THE STAR FORMATION-STELLAR MASS RELATION

Kyle Willett[1], Kevin Schawinski[2], etc.

Draft version September 22, 2014

ABSTRACT

We measure the mass-star formation relation in disk galaxies at $z < 0.05$, using Galaxy Zoo morphologies to examine different populations of spirals as classified by their kiloparsec-scale structure. We examine the number of spiral arms, their average pitch angle, and the presence of a galactic bar in the disk, and show that both the slope and dispersion of the $M_\star$-SFR relation is constant when varying all the above parameters. We also show that mergers (both major and minor), which represent the strongest conditions for increases in star formation at a constant mass, only boost the SFR above the main relation by ~ 0.3 dex; this is a significant reduction over the increase seen in merging systems at $z > 1$. Of the galaxies lying significantly above the $M_\star$-SFR relation in the local Universe, more than 50% are mergers. We interpret this as evidence that the spiral arms, which are imperfect reflections of the galaxy's current gravitational potential, are either fully independent of the various quenching mechanisms or are completely overwhelmed by the combination of outflows and feedback. The arrangement of the star formation can be changed, but the system *as a whole* regulates itself even in the presence of strong dynamical forcing.

Subject headings: galaxies:mergers

1. INTRODUCTION

Observations at a range of redshifts have established that the star formation rate (SFR) of a galaxy is strongly correlated to its stellar mass ($M_\star$). This "star-forming main sequence" (SFMS) is nearly linear and at least at low redshift, has remarkably small scatter (Brinchmann et al. 2004). Recent observations of star-forming galaxies at high redshifts show that this main sequence remains out to high redshift, but with its normalisation shifting up so that galaxies of the same $M_\star$ have a higher SFR at high redshift (Noeske et al. 2007; Daddi et al. 2007). The main sequence has been interpreted by Bouché et al. (2010) and Lilly et al. (2013) as the result of the balancing of inflows of cosmological gas and outflows due the feedback. Galaxies self-regulate to remain in a state of homeostasis as they convert baryons from gas to stars.

As star-forming galaxies exhibit a wide range of physical appearances in optical images, we can ask the natural question of whether the specifics of this physical appearance, and its underlying dynamical processes, have any effect on this homeostasis and therefore the galaxy's location relative to the SFMS. If the details of a galaxy's physical appearance are correlated with position relative to the main sequence, then the dynamical processes that give rise to them – such as bar formation and spiral arm pitch angle – are a fundamental aspect of the galaxy's regulatory mechanism. If, on the other hand, these features are not correlated, then there are two options: either galaxy substructure is simply not relevant to the overall $M_\star$-SFR relationship, or the regulatory mechanism overcomes the local effect of substructure in all circumstances. This ultimately relates to the physical processes that control the overall strength of the regulator in each galaxy.

The fact that star-forming galaxies live on the SFMS is one of the key observations that has been driving the development of new descriptions of how galaxies evolve. Peng et al. (2010, 2012) argue that galaxies grow in stellar mass during their life as star-forming galaxies on the main sequence before being quenched either by an external mechanism (environment or satellite quenching) or by an internal mechanism (mass quenching). This life on the main sequence is thus governed by the action of the regulator balancing gas in- and outflows Lilly et al. (2013), making it the central process in galaxy evolution.

In this paper, we use the Sloan Digital Sky Survey (York et al. 2000; Strauss et al. 2002; Abazajian et al. 2009) in combination with the largest database of visual classifications of galaxy structure and morphology ever assembled from the Galaxy Zoo citizen science projects (Lintott et al. 2008, 2011; Willett et al. 2013) to test whether galaxy structure affects their star formation properties. We use the WMAP9 cosmology parameters of $(\Omega_m, \Omega_\Lambda, h) = (0.258, 0.718, 0.697)$ (Hinshaw et al. 2013).

2. DATA

Data for all galaxies in this paper comes from optical observations in the SDSS DR7. The morphological data is drawn from citizen science classifications in Galaxy Zoo. Merging pairs of galaxies are taken from the catalog of Darg et al. (2010a), all of which lie in the redshift range $0.005 < z < 0.1$. Post-merger spheroidal galaxies without an obvious, separated companion are specifically excluded from the sample. Detailed classifications of disk morphologies, including arm pitch angle, number of spiral arms, and presence of a galactic bar, are taken from the Galaxy Zoo 2 (GZ2) catalog (Willett et al. 2013).

Spiral galaxies are selected according to the following

[1] School of Physics and Astronomy, University of Minnesota, Minneapolis, MN 55455, USA
[2] Institute for Astronomy, Department of Physics, ETH Zürich, Wolfgang-Pauli-Strasse 16, CH-8093, Zürich, Switzerland

TABLE 1
Basic properties of the $M_\star - SFR$ linear fit for GZ2 star-forming galaxies.

Sample	N	α	β	σ_α	σ_β
SF galaxies	52685	0.73	−7.19	5.27×10^{-6}	5.18×10^{-4}
1 arm	39	0.66	−6.31	5.11×10^{-3}	5.14×10^{-1}
2 arms	2914	0.79	−7.74	1.11×10^{-4}	1.14×10^{-2}
3 arms	89	0.57	−5.47	4.17×10^{-3}	4.49×10^{-1}
4 arms	9	0.35	−3.29	9.18×10^{-2}	9.58×10^{0}
5+ arms	9	0.64	−6.88	7.20×10^{-2}	6.91×10^{0}
can't tell	40	0.69	−7.10	1.06×10^{-2}	1.04×10^{0}
tight arms	308	0.73	−7.26	1.68×10^{-3}	1.75×10^{-1}
medium arms	44	0.80	−7.83	5.23×10^{-3}	5.37×10^{-1}
loose arms	470	0.74	−7.14	5.16×10^{-3}	5.18×10^{-2}
barred	4473	0.76	−7.54	7.60×10^{-5}	7.57×10^{-3}
unbarred	11593	0.70	−6.92	2.65×10^{-5}	2.66×10^{-3}
merger	2978	–	−7.91	–	4.40×10^{-4}

Note. — Parameters α and β are fit according to Equation 1.

thresholds in the spectroscopic GZ2 sample, where p is the debiased vote fraction and N the weighted number of total votes: $p_{\rm features/disk} > 0.430$, $p_{\rm not\ edgeon} > 0.715$, $p_{\rm spiral} > 0.619$, and $N_{\rm spiral} > 20$. We identify sub-classes of spiral structure using the morphology flags as given in the GZ2 catalog; these are designed to be conservative cuts, including only robust examples of each morphological class.

Stellar masses and star formation rates are computed from optical diagnostics and taken from the MPA-JHU catalogue (Kauffmann et al. 2003a; Brinchmann et al. 2004; Salim et al. 2007). We use updated masses and activity classifications from the DR7 database.[3] We separate star-forming galaxies from other emission-line galaxies using the standard BPT classification (Baldwin et al. 1981) below the Kauffmann et al. (2003b) demarcation. Galaxies with low signal-to-noise ratio ($S/N > 3$) galaxies are removed. For both $M_\star$ and SFR, we use median values extracted from the PDF.

The total sample analyzed contains 52,685 star-forming galaxies. These are selected from the GZ2 spectroscopic sample with $z < 0.1$, $M_r < -19.5$, and classified as actively star-forming ($BPT = 1$) from the MPA-JHU emission line measurements. The average color for the star-forming galaxies is relatively blue, with $(u-r) = 1.7 \pm 0.6$.

To parametrize the $M_\star - SFR$ relationship, we apply a simple linear model for the total sample and subsamples. We apply a least-squares fit where the data are weighted by the uncertainty in SFR (computed as the mean difference in the 16th and 84th percentiles from the MPA-JHU PDFs). The data are then fit to:

$$\log(SFR) = \alpha(\log[M_\star/M_\odot]) + \beta \qquad [M_\odot/yr] \qquad (1)$$

where α and β represent the slope and offset, respectively. Values of the fits for each subample are given in Table 1; we also provide the formal uncertainties σ_α and σ_β in each parameter from the covariance matrix.

3. RESULTS

We analyze the dependence of the star-forming main sequence for three different sets of disk galaxies: splitting the sample by the observed number (multiplicity) of spiral arms, the relative pitch angle (tightness or winding) of the spiral arms, and the presence of a galactic bar. Both spiral arms and galactic bars can have significant effects on the local properties of a galaxy. Dynamical effects compress gas and trigger recent star formation within spiral arms, while longer galactic bars have redder colors and less star formation than the rest of the disk (Hoyle et al. 2011). We examine whether these kpc-scale effects can be seen long-term in the galaxy's SFR-mass relationship.

For a control sample, we plot in Figures 1-5 the underlying star-forming main sequence relation for star-forming disks as measured in a sample of local SDSS galaxies. As demonstrated in previous papers, there is a fairly tight correlation between $M_\star$ and SFR, with galaxies in the process of quenching lowering their SFR and falling below the trend. The relationship extends over at least 4 orders of magnitude in both $M_\star$ and SFR.

Figure 1 overplots SFR as a function of $M_\star$ for disk galaxies separated by their arm multiplicity. The GZ2 data separates disk galaxies with visible spiral arms into categories of 1, 2, 3, 4, or more than four spiral arms; there is also an additional option if the number of spiral arms cannot be accurately determined. For this analysis, galaxies in each mass/SFR bin is weighted by the vote fraction for the morphology being tested. Two-armed spirals are the most common multiplicity in the GZ2 sample.

The fit to the star-forming main sequence for the six sub-samples of spiral galaxies tightly follows that of that for the total disk population. Both the slopes and offsets of each linear fit are completely consistent within the formal fitting errors (Table 1). There are too few galaxies with reliable spiral morphologies at lower masses to do a reliable fit; however, the same relation is reproduced for all multiplicities at $10^8 < M_\star/M_\odot < 10^{11}$.

The one-armed spirals present an interesting case, with the fit to the weighted population lying slightly *above* that of all star-forming spirals. This is consistent with the work of Casteels et al. (2013), who showed that one-armed spirals in GZ2 are robust indicators of close interactions at projected distances of $r_p < 50\ h^{-1}$ kpc. The underlying reason is that many "one-armed spirals" are in fact caused by bridges or tidal tails from interactions with a nearby companion; we discuss the likely role of merging/interacting galaxies in Figure 5.

The two-armed spirals and those with uncertain multiplicities are the only morphologies that extend slightly below the SFMS. One possibility is that this is a consequence of galaxies that have already begun the process of quenching. As a result, the star-formation rate is depleted and the contrast of spiral arms against the rest of the disk (which for visual identification is at least in part dependent on bright knots of recent star formation) makes the multiplicity more difficult to identify. However, the $(u-r)$ colors of these galaxies (uncorrected for dust extinction) are on average significantly bluer than green-valley late-types as identified in Schawinski et al. (2014).

We have repeated the analysis above for the subsample of disk galaxies for which the spiral multiplicity is determined with high confidence ($p_{\rm arms\ number} > 0.8$) by GZ2, thus eliminating "intermediate" galaxies

[3] http://home.strw.leidenuniv.nl/~jarle/SDSS/

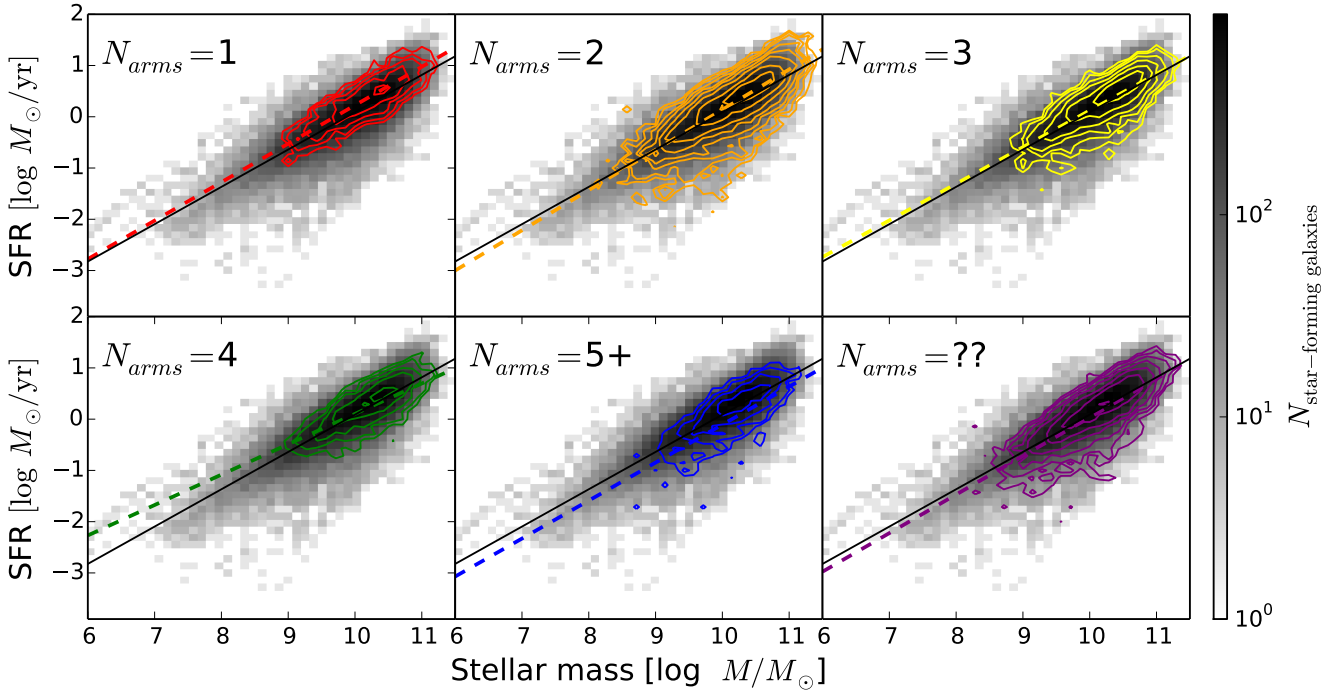

FIG. 1.— Total star formation rate as a function of stellar mass; grayscale colors are the distribution of all star-forming galaxies in SDSS from the MPA-JHU DR7 catalog. Coloured contours in each panel show spiral galaxies weighted by the GZ2 likelihoods of hosting 1, 2, 3, 4, more than four, or "uncertain" numbers of spiral arms, respectively. Dotted lines show the weighted least-squares linear fit to each population as split by arm multiplicity; the solid line is the fit to all of the star-forming galaxies.

for which the morphology is uncertain. These galaxies ($N = 14,148$) is dominated by two-armed spirals, which are the only multiplicity for which significant numbers of galaxies at $M_\star < 10^9\ M_\odot$ are detected. Our results for the SFMS are qualitatively the same as when using the weighting scheme, although we note that there are too few examples ($N < 10$) of either three- or four-armed spirals for a reliable fit. The offset of the one-armed spirals above the SFMS is also significantly more pronounced when using high-confidence morphologies.

The pitch angle of the spiral arms also has no significant change on the star-forming main sequence relation (Figure 2). We separate galaxies by their relative pitch angles (defined as "tight", "medium", and "loose"); the pitch angle is typically used as one of the primary drivers for separating galaxies along the Hubble tuning fork. Willett et al. (2013) show, however, that pitch angle only weakly correlates with Hubble type from expert visual classifications, and that the bulge-to-disk ratio is a more important driver. All three categories correlate tightly with spiral galaxies in general; we note that the small deviation above the main sequence for loosely-wound galaxies is also consistent with Casteels et al. (2013), who show that this morphology also correlates with close pairs and interactions.

It should also be noted that the galaxies in GZ2 flagged as a function of pitch angle are not representative of the true vote distribution. The raw numbers in Figure 2 suggest that most spiral galaxies are either tightly or loosely wound. In fact, the plurality classification for most galaxies is for medium-winding; the spread in votes is typically large, though, and so users rarely agree on the medium option at the 80% level which sets the flag. We have extended this analysis by plotting the same star-forming main sequence diagram as a function of $p_{\rm arms\ winding}$, which more accurately tracks the pitch angle distribution. In this case, it also closely follows the main star-forming main sequence (Figure 6).

Finally, we examine the effect of a large-scale galactic bar on the star-forming main sequence. This sample is significantly larger than those including spiral arm morphology, since the classification is at a higher level in the GZ2 tree and has only two choices; this results in a higher percentage of consensus classifications that set the flag. Figure 3 shows the star-forming main sequence for both barred and unbarred galaxies. Although the fraction of barred galaxies potentially varies as a function of stellar mass (Masters et al. 2011; Cheung et al. 2013), both the linear fits and ranges of the sub-populations are consistent with all star-forming galaxies. In other words, the presence of a bar does not affect the galaxy's position on the star-forming main sequence.

The agreement of all sub-varieties of star-forming galaxies is supported by the close agreement to the linear fits to the data for all well-sampled categories (Table 1). This tracks only the slope and offset of the distribution, however, and not its width. We thus also compared the sample standard deviation (σ_{SFR}) as a function of mass of the star-forming galaxy population to its various subsamples. The value of σ_{SFR} monotonically decreases with mass over the range $6.0 < \log(M/M_\odot) < 11.5$. For all populations examined in this paper, though,

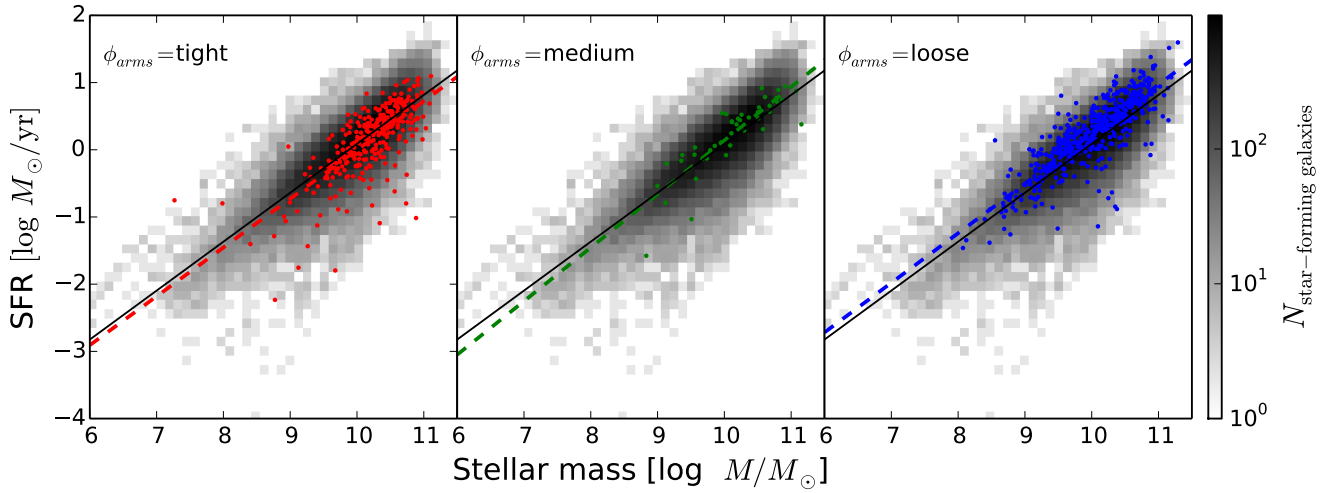

FIG. 2.— Total star formation rate as a function of stellar mass; grayscale colors are the same as in Figure 1. From left to right: red, green, and blue points are spiral galaxies with "tight", "medium", and "loose" winding spiral arms as identified by GZ2 morphology flags. Dotted lines show the weighted least-squares linear fit as split by pitch angle; the solid line is the fit to all star-forming galaxies.

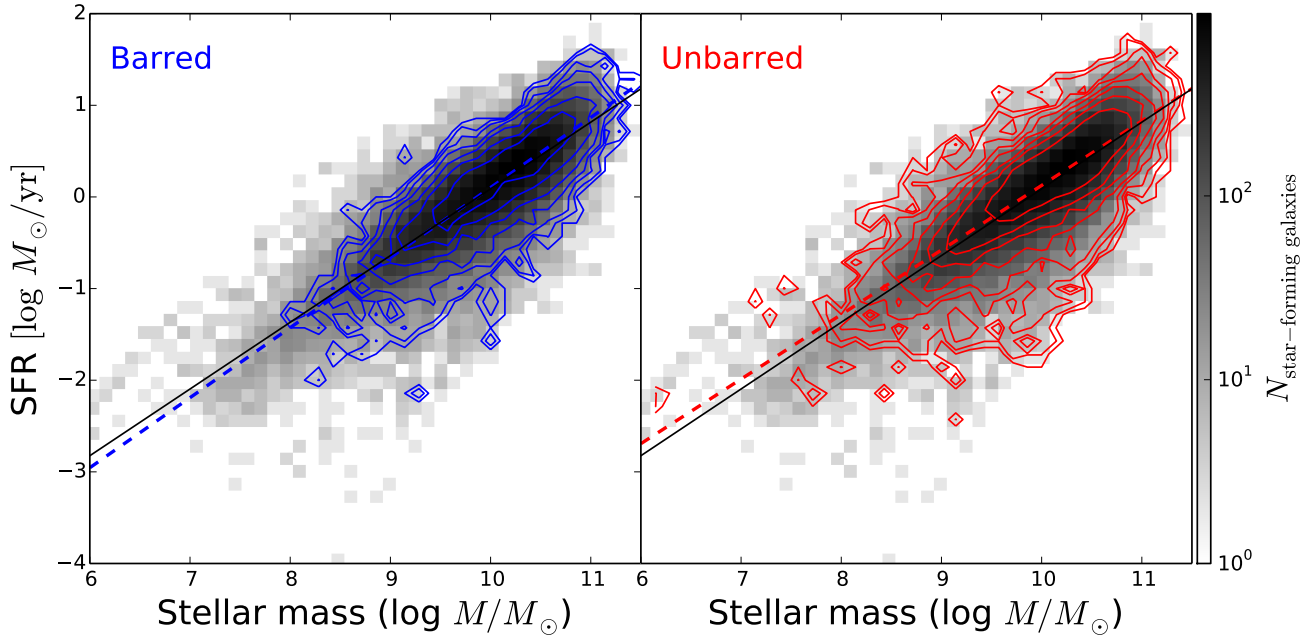

FIG. 3.— Total star formation rate as a function of stellar mass; grayscale colors are the same as in Figure 1. Left: blue contours show the distribution of barred galaxies ($p_{\rm bar} \geq 0.4$ for previously-identified disks) from GZ2. Right: red contours are the distribution of remaining disk galaxy population with no evidence for a strong bar ($p_{\rm bar} < 0.4$). Dotted lines show the weighted least-squares linear fit to the barred/unbarred population; the solid line is the fit to all star-forming galaxies.

the widths of their distributions are consistent with the broader population (Figure 4).

We have examined all the populations of galaxies described above (bars, arm pitch angle, arm multiplicity) and measured the differences when using specific star formation rate (sSFR $\equiv$ SFR/$M_\star$) instead of SFR. There is no significant change in the results.

4. DISCUSSION

Our results show that the star-forming main sequence is remarkably robust to the details of the spatial distribution of star formation *within* galaxies. Testing for a wide range of morphological sub-types of star-forming disk galaxies yields no statistically significant difference in the relative position of these sub-types vis-á-vis the main sequence. Neither the number or pitch angle of spiral arms, or the presence of a large-scale bar are correlated with any detectable increase or decrease in the efficiency of star formation. The system which regulates star formation in galaxies is thus either not affected by the details of the spatial distribution of star formation,

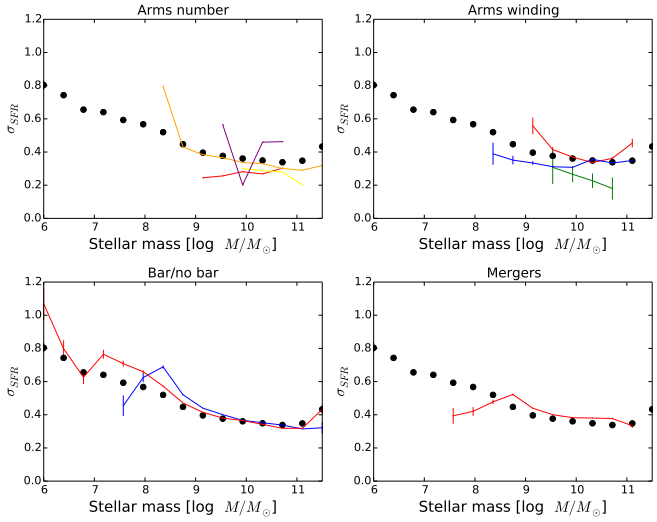

FIG. 4.— Width of the star-forming main sequence (σ) as a function of stellar mass, as measured by the sample standard deviation. Black points represent the entire star-forming population. The various disk subsamples are overplotted as lines; colours are the same as the respective plots in Figures 1-3 and 5. Morphological categories or mass ranges with fewer than 10 galaxies/bin are not plotted; this includes all mass ranges for 3-, 4-, and more than 4-armed spirals.

or its regulatory effect is so strong that it wipes out any such effect in a short time.

Abramson et al. (2014) found that by normalizing galaxies by the stellar mass of the disk alone, the slope of the SFMS is consistent with only a linear trend (removing any dependence on mass). Although this correction to the disk stellar mass homogenizes the SFMS for disks with a range of B/T, the dispersion (σ_{SFR}) of the sequence must be a result of contributions by bars, disk dynamics, halo heating, AGN activity, and/or environment (among other factors). Our results show that the neither of the first two factors play dominant roles in controlling σ_{SFR}, at least as far as major dynamical drivers (such as strong bars or additional arms) are concerned. Thus while the overall bulge strength does affect the position of a galaxy on the SFMS (Martig et al. 2009; Chevance et al. 2012; Fang et al. 2013; Kaviraj 2014; Lang et al. 2014; Omand et al. 2014), the structure of the *disk itself* does not.

The lack of any difference in SFR as a function of mass for barred vs. unbarred galaxies is in general agreement with Ellison et al. (2011), who find an increase of Δ SFR ~ 0.15 dex, but only for galaxies with $M_\star > 10^{10.7}\ M_\odot$. This is at the very upper end of the mass range probed in Figure 3. If the increase in star formation is limited to the central kpc of the disk (as they demonstrate using fibre SFR measurements), an increase in possible bar-driven SFR increase is seen down to $M_\star = 10^{10}\ M_\odot$.

Amongst individual galaxies that lie significantly off the SFMS, compact starburst galaxies show the largest increase in SFR at a given mass (Elbaz et al. 2011). In the local Universe, these include optically-identified "green pea" galaxies, which have unusually high sSFR and can lie more than 1 dex above the SFMS (Cardamone et al. 2009). While few known green pea galaxies have detailed imaging available, their most common morphology is in a clumpy arrangement with knots of bright star formation. There is thus little evidence for a dynamically-settled disk (in any arrangment) for galaxies in the local Universe lying significantly above the SFMS.

As a comparison to the kpc-scale structures discussed above, we analyze the impact of the most significant forcing event to a galaxy system known – a major galaxy merger (Figure 5). In these systems (which are in various stages of coalescence) the star formation rates are increased by only an average of 0.29 dex, corresponding to less than a factor of two overall. Darg et al. (2010b) showed that in the local ($z < 0.1$) Universe, galaxies with intense bursts of star formation are limited to only the spiral (disc) galaxies. This increase in star formation for mergers does show a strong evolution in redshift out to at least $1.5 < z < 2.5$, likely due to the higher gas fractions involved (Daddi et al. 2010; Rodighiero et al. 2011). The projected separation between galaxies in which this occurs, based on both the observed merger fraction and sSFR is ~ 0.1 Mpc/h (Skibba et al. 2009). Our measurements are consistent with observations of galaxies at $z \simeq 2$ (Kaviraj et al. 2013), which support a merger-driven increase of only a factor of ~ 2 in sSFR.

The location of mergers on the present-day SFMS shows just how stable the regulatory system in galaxies really is. Almost all simulations of galaxy mergers predict a steep increase in the star formation rate during both first passage and final coalescence (eg, Hopkins et al. 2008). The magnitude of this increase often depends on the details of the simulation, but can range from a factor of 10 to 100. Observations of mergers in Stripe 82 data, however, limit this increase to between a factor of 2 and 6 (Kaviraj 2014). In the low-redshift universe sampled by SDSS and Galaxy Zoo, we also find no evidence for an enhancement more than an order of magnitude. This in turn suggests that the current generation of galaxy merger simulations misses critical feedback mechanisms that prevent runaway peaks in star formation rates during mergers.

5. CONCLUSIONS

We analyze for the first time the detailed structure of disks in star-forming galaxies as related to their position on the $M_\star$-SFR relation, using morphological classifications from the Galaxy Zoo 2 project. We find that neither the slope nor the dispersion of the star-forming galaxies are affected when splitting the sample into different categories of disks, including barred/unbarred galaxies, the pitch angle of spiral arms, or the number of spiral arms.

The uniformity of disk galaxies along the SFMS, regardless of their kpc-scale structure, argues for the system as a whole being strongly self-regulated. While smaller regions of the galaxy can experience (likely temporary) increases in star formation, the amount of star formation in the disk as a whole is conserved. This is preserved even for the strongest forcing events, including major mergers; the physics governing the SFMS are primarily driven by the overall mass of the system. This means that simulations of galaxy evolution must be able to meet the challenge of simultaneously reproducing the wide range of disk morphologies observed along the Hubble sequence (and in various merger stages) while simultaneously managing feedback so that *all* disk types maintain the same tight relationship to the SFMS.

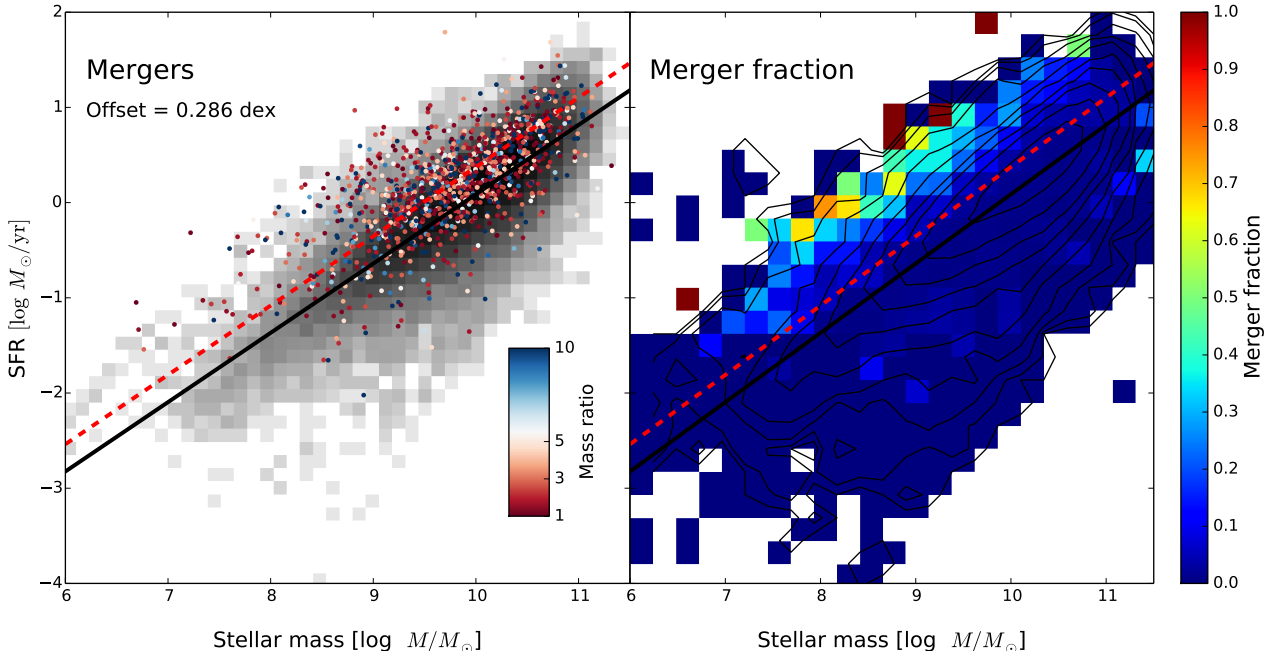

FIG. 5.— Total star formation rate as a function of stellar mass; grayscale colors are the same as in Figure 1. Left: Coloured points show 2,978 merging galaxies from Darg et al. (2010a). Mergers are colour-coded by the mass ratio of the primary and secondary galaxies; there is no clear difference in the merging populations with regard to the SFMS when comparing major to minor mergers. When fixing the slope of the star-forming main sequence and allowing the offset to vary, mergers (dotted line) have higher SFRs by ~ 0.3 dex compared to all star-forming galaxies (solid line). Right: Star-forming galaxies binned and colour-coded by merger fraction ($N_{\rm mergers}/N_{\rm star\text{-}forming\ galaxies}$). Overplotted lines are the same as left plot. Of the galaxies that lie furthest above the SFMS, more than 50% are unambiguous mergers.

The data in this paper are the result of the efforts of the Galaxy Zoo volunteers, without whom none of this work would be possible. Their efforts are individually acknowledged at http://authors.galaxyzoo.org. Please contact the authors to request access to research materials discussed in this paper.

We thank Rory Smith and Lucio Mayer for useful discussions. This research made use of TOPCAT, an interactive graphical viewer and editor for tabular data (Taylor 2005) and Astropy, a community-developed core Python package for astronomy (Astropy Collaboration et al. 2013).

KS gratefully acknowledges support from Swiss National Science Foundation Grant PP00P2_138979/1.

Funding for the SDSS and SDSS-II has been provided by the Alfred P. Sloan Foundation, the Participating Institutions, the National Science Foundation, the U.S. Department of Energy, the National Aeronautics and Space Administration, the Japanese Monbukagakusho, the Max Planck Society, and the Higher Education Funding Council for England. The SDSS website is http://www.sdss.org/.

The SDSS is managed by the Astrophysical Research Consortium for the Participating Institutions. The Participating Institutions are the American Museum of Natural History, Astrophysical Institute Potsdam, University of Basel, University of Cambridge, Case Western Reserve University, University of Chicago, Drexel University, Fermilab, the Institute for Advanced Study, the Japan Participation Group, Johns Hopkins University, the Joint Institute for Nuclear Astrophysics, the Kavli Institute for Particle Astrophysics and Cosmology, the Korean Scientist Group, the Chinese Academy of Sciences (LAMOST), Los Alamos National Laboratory, the Max-Planck-Institute for Astronomy (MPIA), the Max-Planck-Institute for Astrophysics (MPA), New Mexico State University, Ohio State University, University of Pittsburgh, University of Portsmouth, Princeton University, the United States Naval Observatory, and the University of Washington.

REFERENCES

Abazajian, K. N., Adelman-McCarthy, J. K., Agüeros, M. A., et al. 2009, ApJS, 182, 543
Abramson, L. E., Kelson, D. D., Dressler, A., et al. 2014, ApJ, 785, L36
Astropy Collaboration, Robitaille, T. P., Tollerud, E. J., et al. 2013, A&A, 558, A33
Baldwin, J. A., Phillips, M. M., & Terlevich, R. 1981, PASP, 93, 5
Bouché, N., Dekel, A., Genzel, R., et al. 2010, ApJ, 718, 1001
Brinchmann, J., Charlot, S., White, S. D. M., et al. 2004, MNRAS, 351, 1151
Cardamone, C., Schawinski, K., Sarzi, M., et al. 2009, MNRAS, 399, 1191
Casteels, K. R. V., Bamford, S. P., Skibba, R. A., et al. 2013, MNRAS, 429, 1051
Cheung, E., Athanassoula, E., Masters, K. L., et al. 2013, ApJ, 779, 162
Chevance, M., Weijmans, A.-M., Damjanov, I., et al. 2012, ApJ, 754, L24
Daddi, E., Dickinson, M., Morrison, G., et al. 2007, ApJ, 670, 156
Daddi, E., Elbaz, D., Walter, F., et al. 2010, ApJ, 714, L118
Darg, D. W., Kaviraj, S., Lintott, C. J., et al. 2010a, MNRAS, 401, 1043
—. 2010b, MNRAS, 401, 1552
Elbaz, D., Dickinson, M., Hwang, H. S., et al. 2011, A&A, 533, A119
Ellison, S. L., Nair, P., Patton, D. R., et al. 2011, MNRAS, 416, 2182

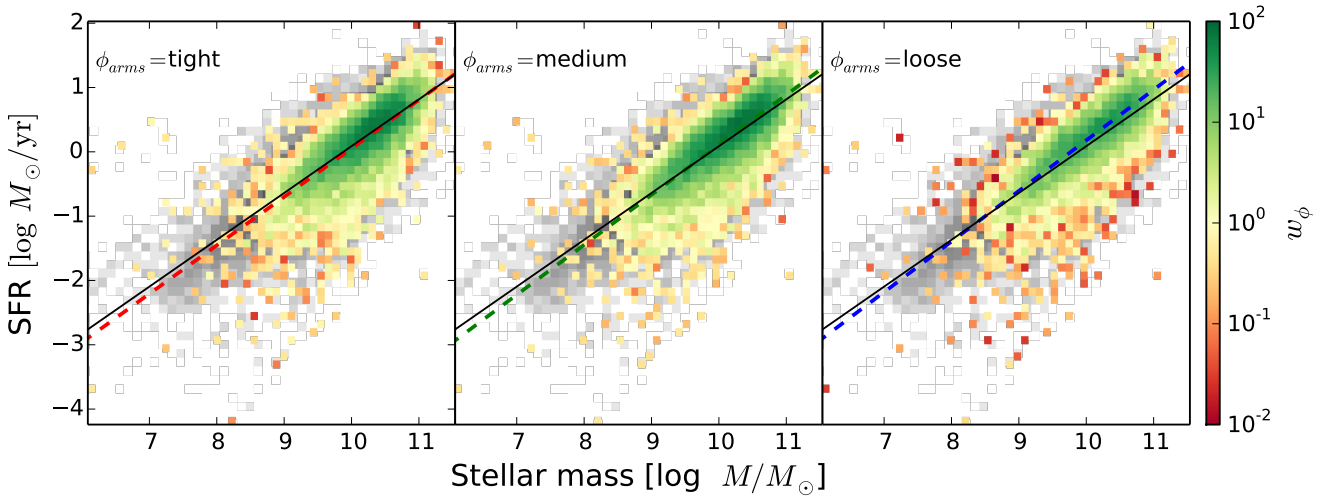

FIG. 6.— Total star formation rate as a function of stellar mass; grayscale colors are the same as in Figure 2. From left to right: colormaps show spiral galaxies weighted by the GZ2 vote fractions for "tight", "medium", and "loose" winding spiral arms. Dotted lines show the weighted least-squares linear fit as split by pitch angle; the solid line is the fit to all star-forming galaxies.

Fang, J. J., Faber, S. M., Koo, D. C., & Dekel, A. 2013, ApJ, 776, 63

Hinshaw, G., Larson, D., Komatsu, E., et al. 2013, ApJS, 208, 19

Hopkins, P. F., Hernquist, L., Cox, T. J., & Kereš, D. 2008, ApJS, 175, 356

Hoyle, B., Masters, K. L., Nichol, R. C., et al. 2011, MNRAS, 415, 3627

Kauffmann, G., Heckman, T. M., White, S. D. M., et al. 2003a, MNRAS, 341, 33

Kauffmann, G., Heckman, T. M., Tremonti, C., et al. 2003b, MNRAS, 346, 1055

Kaviraj, S. 2014, MNRAS, 440, 2944

Kaviraj, S., Cohen, S., Windhorst, R. A., et al. 2013, MNRAS, 429, L40

Lang, P., Wuyts, S., Somerville, R. S., et al. 2014, ApJ, 788, 11

Lilly, S. J., Carollo, C. M., Pipino, A., Renzini, A., & Peng, Y. 2013, ApJ, 772, 119

Lintott, C., Schawinski, K., Bamford, S., et al. 2011, MNRAS, 410, 166

Lintott, C. J., Schawinski, K., Slosar, A., et al. 2008, MNRAS, 389, 1179

Martig, M., Bournaud, F., Teyssier, R., & Dekel, A. 2009, ApJ, 707, 250

Masters, K. L., Nichol, R. C., Hoyle, B., et al. 2011, MNRAS, 411, 2026

Noeske, K. G., Weiner, B. J., Faber, S. M., et al. 2007, ApJ, 660, L43

Omand, C. M. B., Balogh, M. L., & Poggianti, B. M. 2014, MNRAS, 440, 843

Peng, Y.-j., Lilly, S. J., Renzini, A., & Carollo, M. 2012, ApJ, 757, 4

Peng, Y.-j., Lilly, S. J., Kovač, K., et al. 2010, ApJ, 721, 193

Rodighiero, G., Daddi, E., Baronchelli, I., et al. 2011, ApJ, 739, L40

Salim, S., Rich, R. M., Charlot, S., et al. 2007, ApJS, 173, 267

Schawinski, K., Urry, C. M., Simmons, B. D., et al. 2014, MNRAS, 440, 889

Skibba, R. A., Bamford, S. P., Nichol, R. C., et al. 2009, MNRAS, 399, 966

Strauss, M. A., Weinberg, D. H., Lupton, R. H., et al. 2002, AJ, 124, 1810

Taylor, M. B. 2005, in Astronomical Society of the Pacific Conference Series, Vol. 347, Astronomical Data Analysis Software and Systems XIV, ed. P. Shopbell, M. Britton, & R. Ebert, 29

Willett, K. W., Lintott, C. J., Bamford, S. P., et al. 2013, MNRAS, 435, 2835

York, D. G., Adelman, J., Anderson, Jr., J. E., et al. 2000, AJ, 120, 1579

APPENDIX